ORIGINAL PAPER

Atmospheric Plasma Supported by TiO$_2$ Catalyst for Decolourisation of Reactive Orange 16 Dye in Water

Tatjana Mitrović[1] · Nataša Tomić[2] · Aleksandra Djukić-Vuković[3] · Zorana Dohčević-Mitrović[4] · Saša Lazović[2]

Abstract

Purpose Every advanced oxidation process (AOP) has its limitations in water purification. Novel designs with simultaneous application of different AOPs can offer better solutions for cleaner water.

Methods We have comparatively studied two advanced oxidation processes (AOPs) on decolourisation of Reactive Orange 16 (RO 16) azo dye pollutant from water: gas plasma treatment by low power atmospheric pressure plasma using novel plasma needle configuration, and semiconductor heterogeneous photocatalysis using titanium dioxide (TiO$_2$) nanopowders. Additionally, simultaneous application of two advanced oxidation processes on azo dye decolourisation was studied.

Results It was found that plasma treatment is very efficient system for the dye removal even for low flow rates (1 slm) of the Ar as feed gas. The presence of 10% of O$_2$ in Ar flow intensified dye oxidation process and shortened required time for total decolourisation. When plasma and catalyst were simultaneously applied, TiO$_2$ was activated with a few Watts plasma source as well as 300 W UV lamp source. The synergic effect of two AOPs was more pronounced for higher feed gas flow rates, resulting in improved decolourisation efficiency.

Conclusion Plasma needle can efficiently remove Reactive Orange 16 azo dye from water with a power consumption of only few Watts. With the addition of TiO$_2$ the removal efficiency is significantly improved.

Graphic Abstract
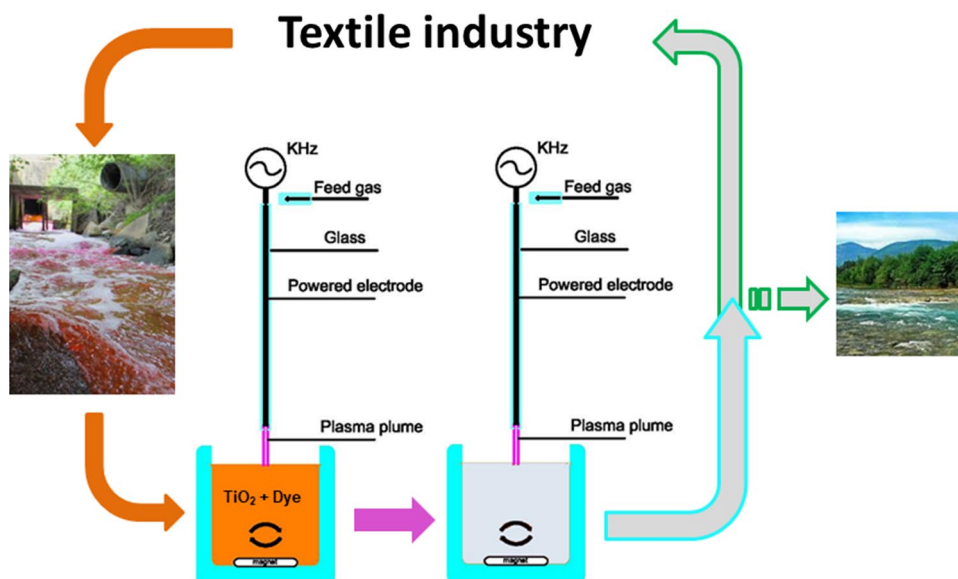
Extended author information available on the last page of the article

Statement of Novelty

Textile industry consumes around 2000 L of water to produce a single pair of jeans. Ten to fifteen percent of the global production of dyes is discharged into the waterbodies. This is not sustainable. Treated wastewater has to be reused. We propose a novel and efficient method for treatment of textile industry wastewater. A combination of two advanced oxidation processes—low power atmospheric pressure plasma and TiO_2 heterogeneous photocatalysis is used for decolourisation of Reactive Orange 16 azo dye pollutant.

Introduction

Since water is one of the most important resources, its availability and quality have become one of the biggest social priorities today. Increasing pollution of the water system, including textile industries and agriculture, affects ecosystem and human health directly and represent the widespread concern.

Textile and paper industries generate complex and diverse effluents and they belong to the most polluting industrial sectors [1]. Organic dyes as the main components of these effluents, are considered to be very toxic, mutagenic, and potentially carcinogenic [2, 3]. About 10–15% of the total world production of dyes are discharged into different waterbodies affecting directly aquatic life by disrupting the amount of dissolved O_2 and consequently photosynthesis and respiration processes [4-6].

Azo dyes are organic molecules generally with an azo bond (R–N $=$ N–R') as main chromophore group. They are widely used in textile industry and because of their chemical complexity and low biodegradability; the wastewater treatment is very demanding. Different methods are applied to remove these organic compounds from the water sources: biological, physicochemical (adsorption, coagulation/flocculation, reverse osmosis) or chemical treatments (chlorination and ozonation). However, these methods have certain limitations. The biological treatments are not effective in the case of stable and resistant azo dyes. Only few unstable azo dyes can be degraded under aerobic conditions. On the other hand, anaerobic degradation causes aromatic amines generation which are toxic and carcinogenic [7]. The physicochemical treatments often cause formation of secondary pollution, generating large amounts of sludge and transferring pollutants from water to solid phase. Therefore, incomplete degradation and necessity for additional operations including final degradation of

the waste and adsorbent regeneration limit the application of these treatments [8]. Chemical treatments like chlorination can result in complete decolourisation of dyes, but chlorinated organic by-products are very hazardous [9]. Ozone oxidizes dyes as well, but its extreme oxidizing effects can harm the atmosphere. Thus, ozonation system must include a control unit which prevents excessive use of chemicals [10].

Advanced oxidation processes (AOPs) have shown some advantages over the conventional water purification technologies. Based on the production of very strong and unselective oxidizing species (hydroxyl radicals—$OH^.$), these techniques are used in mineralization of soluble complex organic pollutants. The ultimate goal of this process is to decompose pollutants to CO_2, H_2O, and some inorganic ions. Most common AOPs are: gas plasma oxidation [11, 12], (heterogeneous) photocatalytic oxidation [13, 14], ultrasounds [15], photo Fenton oxidation [16, 17], etc.

Among above-mentioned treatments, gas plasma is a relatively novel AOP method for wastewater decontamination. The method is based on ionized gas produced by an electrical discharge, generating electrons, radicals ($OH^.$, $H^.$, $O^.$), ions ($OH-$, H_2O+, $H+$, HO_2^-) and neutrals (H_2O_2, O_3). Plasma systems can be generally divided into thermal or non–thermal plasma. Thermal plasma typically needs more power than non–thermal and creates high flux of heat, which can be used for degradation of very resistant organic molecules. In the case of non–thermal plasma, electrons are at temperatures as high as 11,000 K, and are colliding with gas molecules at temperatures as low as the room temperature, promoting the generation of chemically active species [18].

Previous studies reported that non-thermal plasma generated in the gas phase above the water surface initiates many chemical and physical effects including a high electric field, intense ultraviolet radiation, overpressure shock waves and, of particular importance, formation of various chemically strong oxidative species like radicals and molecules ($OH^.$, $H^.$, $O_2^{.-}$, $O^.$, H_2O_2, O_3). These species, dissolved in water, initiate oxidation processes [19, 20].

Until now, various types of non–thermal plasma devices such as plasma jets [21, 22], plasma needle [23-25], gliding arc [26, 27], dielectric barrier discharge [28, 29], pulsed corona discharges [30, 31] have been developed. These systems have strong oxidizing ability and include simple feed conditions such as temperature and atmospheric pressure. During the treatment, various complex chemical reactions (collision, addition, dissociation and transformation reactions) can be initiated in the polluted solution [26]. Among above mentioned types of non-thermal plasma devices, plasma needle may be easily operated under atmospheric pressure and room temperature and do not require expensive vacuum systems. Its simple configuration provides very easy to work and it can be applied to a

wide range of vessels for treatment. Plasma needle is non-aggressive oxidation method which produces chemically active species at low gas temperature, thus meets all the necessary conditions for the treatment of organic materials, living tissues (wound sterilization, cancer treatment and other biomedical applications) and delicate materials which are unable to withstand vacuum or are thermally sensitive (heat- sensitive polymers, foodstuffs).

Liquid and gas plasma chemistry have been largely studied during the last decade and it is concluded that the degradation takes place mainly because of the formation of reactive radicals. The amount of radicals and their oxidation mechanisms depend on the discharge type and properties, such as the feed gas composition and flow rate, but also on the properties of the liquid [32]. Since the efficiency of non–thermal plasma treatment is highly dependent on the characteristics of both contaminant and liquid media, it is necessary to study and develop adequate treatment scheme for every pollutant/wastewater system.

Another most explored AOP is heterogeneous photocatalysis, because it is suitable for the destruction of resistant hazardous contaminants, as it uses inexpensive operational parameters such as light and semiconductors [33, 34]. It is based on the application of semiconductors and their capability to generate electron–hole pairs under light irradiation, which participate in different redox reactions on the catalyst surface leading to mineralization of the pollutant.

Nowadays, one of the most promising treatments for wastewater remediation combines plasma treatment with metal oxide catalysts [35]. The most common catalysts reported in literature are: TiO_2 [8, 36-38], ZnO [39], Fe_2O_3 [40], NiO [41], and Al_2O_3 [42]. It is expected that combined plasma—catalyst treatment can overcome drawbacks of individual plasma treatment and photocatalysis, preventing at the same time the electron–hole recombination at metal oxide surface and enhancing the mass transport of the reactants to the solid surface [18].

In this paper, we have investigated the decolourisation of toxic RO 16 azo dye through different treatments: low power atmospheric pressure gas plasma (plasma needle configuration); heterogeneous photocatalysis using TiO_2 as catalyst; and combined plasma–catalysis application. To the best of our knowledge, the joint application of plasma needle and catalyst employed for decolourisation of organic dye has not been studied yet. We have developed plasma needle setup to study the effects of flow rate, feed gas composition (Ar and Ar/O_2 mixture), and the eventual UV influence on the oxidation process. Furthermore, we attempted to enhance the efficiency of the decolourization process by combining plasma and TiO_2 photocatalyst and to evaluate the synergic effect of non–thermal plasma and TiO_2 for the decomposition of RO 16 in aqueous solution.

Experimental Section

Chemicals and Sample Preparation

RO 16 (C.I. 17,757; CAS 20262–58–2; $C_{20}H_{17}N_3O_{11}S_3Na_2$, Sigma Aldrich) was used as a model pollutant. The TiO_2 nanopowders were prepared by a sol–gel method using tetrabutyltitanate (Ti $(OBu)_4$) as a precursor, hydrochloride acid as the catalyst, ethanol as the solvent and water for the hydrolysis. The hydrolysis and polycondensation reactions of $Ti(OBu)_4$ were carried out on the ice–bath. The reagent molar ratio was $Ti(OBu)_4$:HCl:EtOH:H_2O = 1:0.3:15:4 [43]. After the gelation, the wet gel was dried at 80 °C, and then calcinated at 500 °C for 1.5 h.

TiO$_2$ Characterization

Phase identification of TiO_2 sample was performed by X–ray powder diffraction (XRPD) (Ital Structures APD2000, Italy) using Cu–Kα radiation (λ = 1.5406 Å). The measurements were performed at room temperature in the 2θ range from 20 to 80º in a continuous scan mode with a step width of 0.1° and the counting time of 0.5 s/step. Software MDI Jade 5.0 was used for the calculation of the structural and microstructural parameters. The powder specific surface area of the sample was calculated following the multipoint BET procedure on the Quantachrome ChemBet-3000 setup. The nitrogen adsorption–desorption isotherm was obtained at 77 K. Morphology of the synthesized nanopowders has been studied on a Tescan MIRA3 field emission gun scanning electron microscope (FE-SEM), at 20 kV in high vacuum. The infrared (IR) transmission spectrum of TiO_2 using the potassium bromide pellet was measured on a Thermo Nicolet 6700 Fourier transform infrared spectrophotometer at the room temperature.

Treatment Setups

In Fig. 1 five different treatment setups are presented: plasma treatment – PT (Fig. 1a), PT with quartz glass (Fig. 1b), heterogeneous photocatalysis–HP (Fig. 1c), plasma coupled with catalyst—PC (Fig. 1d) and PC with quartz glass (Fig. 1e).

The plasma needle setup, which we have adapted for this research (Fig. 1a), consists of a body made of Teflon and a central copper electrode inserted in the glass tube 1 mm above the sample. Its electrical properties are presented by Zaplotnik et al. [44]. Discharge is generated at the tip of a copper wire. Ar (5.0 purity) and a mixture of Ar and O_2 ($Ar/10\%O_2$) are used as feed gases. The flow rates vary from
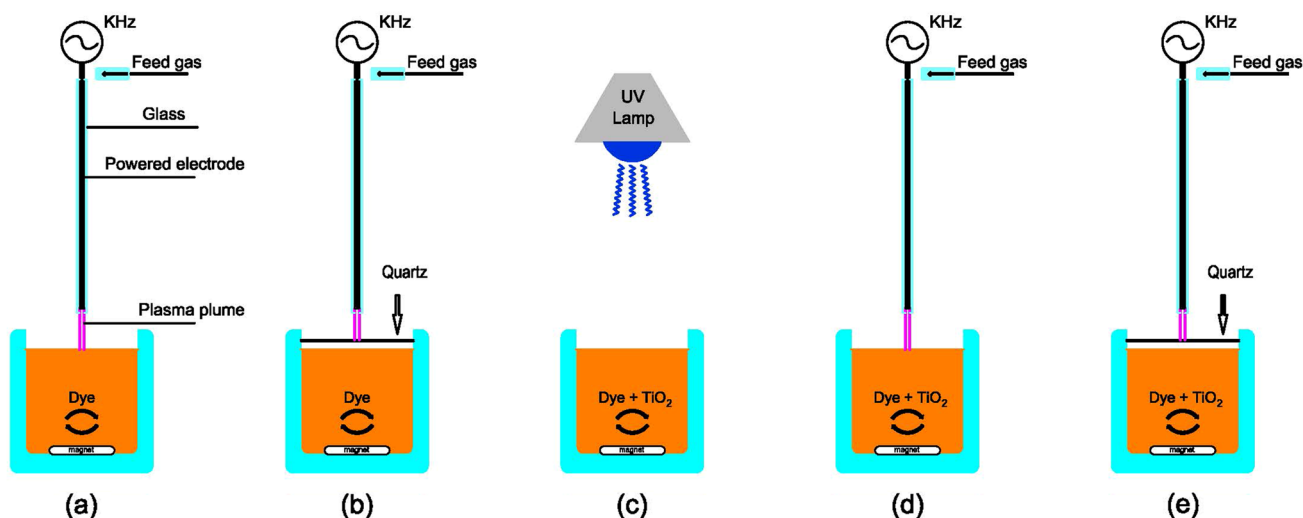
Fig. 1 Different treatment setups used in the study: **a** Plasma treatment (PT), **b** Plasma treatment (PT) with quartz glass, **c** semiconductor heterogeneous photocatalysis (HP), **d** plasma coupled with catalyst (PC), **e** plasma coupled with catalyst (PC) with quartz glass

1 to 4 slm. The exposure times for all treatments range from 5 to 150 min.

In the first set of experiments (PT, Fig. 1a) we have analysed the decolourisation effects of plasma needle on the RO 16 solution, by changing its flow rate and feed gas composition. UV contribution of plasma needle to decolourisation process was investigated by putting a quartz glass (190 to 2500 nm) between the sample and the plasma source (Fig. 1b). In such a way only UV contribution from plasma source to the decolourisation process can be estimated, as in this configuration reactive radicals generated in plasma are prevented to reach the sample surface and oxidize the dye.

The photocatalytic experiment (Fig. 1c) was performed as follows: TiO$_2$ (2 g/l as the optimal concentration for RO 16 photodegradation) [13] was added to the RO 16 solution and magnetically stirred for 30 min in the dark in order to uniformly disperse nanopowder and to achieve the adsorption–desorption equilibrium. Afterwards, a mercury lamp (300 W, UVA/UVB, Osram Vitalux) as a light source placed 40 cm above the sample was switched on in order to initiate the photocatalytic reaction.

In the third set of experiments, we have used plasma needle in the presence of TiO$_2$ (Fig. 1d) in order to examine whether there is a synergic oxidation outcome. The effects of plasma generated UV radiation on the TiO$_2$ activation was investigated by using quartz glass in order to restrict reactive radicals to participate in the dye oxidation process (Fig. 1e).

Decolourisation Measurements

The above–mentioned experiments were conducted in magnetically stirred thermostated glass vessel. The concentration of dye solution (c = 50 mg/l) and working volume

(V = 25 ml) were kept fixed during all treatments. At certain time intervals, aliquots were withdrawn, centrifuged (in the case of TiO$_2$) and analysed on UV/VIS spectrophotometer (Varian Superscan 3, USA). RO 16 concentration was followed by measuring the variation of the intensity of main absorption band at 494 nm. This absorption band originates from n$\rightarrow\pi$* transition in the chromophore group (–N=N–) and its disappearance indicates that the main chromophores of the dye were destroyed. The measurements were repeated three times to check their reproducibility and the mean value was taken into consideration.

Detection of Reactive Hydroxyl Radicals

In order to detect the formation of free hydroxyl radicals, photoluminescence (PL) measurements were performed using terephthalic acid (TA), which in reaction with hydroxyl radicals induced on the photocatalysts surface produces highly fluorescent 2-hydroxyterephthalic acid. The experiment was carried out at room temperature, where 20 mL of working solution was prepared using distilled water in such a manner that the concentrations of the terephthalic acid (TA) and NaOH were 5×10^{-4} M and 2×10^{-3} M, respectively. The nanopowder TiO$_2$ (50 mg) was dispersed and solution was constantly stirred on a magnetic stirrer. A 300 W UV lamp, (Osram Vitalux) was used as a light source, placed 40 cm above the solution. At given time intervals (5, 10, 15, 20 and 30 min), aliquots were withdrawn, centrifuged and filtered to remove the catalyst particles. The room-temperature PL spectra at 425 nm of the supernatant were analyzed on the Fluorescence Spectrometer (Spex Fluorolog) using 320 nm as excitation light, in order to estimate the concentration of 2-hydroxyterephthalic acid.

Results and Discussion

The RO 16 decolourisation mechanism by plasma needle is dependent on the generation of plasma directly above the treated sample in the continuous gas phase simultaneously contacting molecules, clusters, aerosols, droplets, and planar surfaces of the liquid [45]. The complexity of physical and chemical phenomena, which appear during the discharges in both gas and liquid phase, is considerable. For this reason, we studied different plasma needle treatment parameters (e.g. feed gas flow rate and composition) and their influence on the RO 16 oxidation process (decolourisation). Later, we have also studied combined plasma–heterogeneous photocatalysis in order to examine the potential oxidation synergic effects of plasma and catalyst and to verify whether plasma UV radiation was adequate to activate the TiO_2 surface. The TiO_2 based heterogeneous photocatalysis on RO 16 degradation was used as a benchmark.

Effects of Plasma Treatment on the RO 16 Decolourisation

Producing concurrently large amount of active species with high reduction potential (Table 1) [46] UV radiation and shock waves, plasma decomposes organic matter with no additional procedures and no sludge production [47]. Chemically reactive radicals reach the liquid surface, diffuse into the bulk, and oxidize the hazardous component. Therefore, plasma chemistry, which occurs in these atmospheric and subsequently aqueous conditions, is highly relevant to the evolution of the reactive radicals and their influence on the target compound. Figure 2 illustrates the formation mechanisms of possible reactive species, whereas the oxidation potential of plasma reactive species are given in Table 1.

Key reactions from Fig. 2 which take place during the air discharge are described in the following sections.

Depending on the electron energies formed by electrical discharges, high–energy electrons collide with ambient molecules resulting in the several possible reactions such as excitation, dissociation, electron capture or ionization, (Eqs. 1–5):
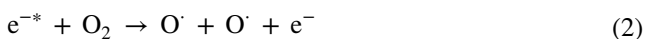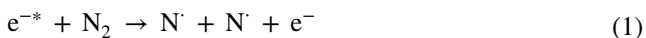
$$e^{-*} + N_2 \rightarrow N^{\cdot} + N^{\cdot} + e^- \tag{1}$$

$$e^{-*} + O_2 \rightarrow O^{\cdot} + O^{\cdot} + e^- \tag{2}$$

Table 1 Oxidation potential of plasma reactive species

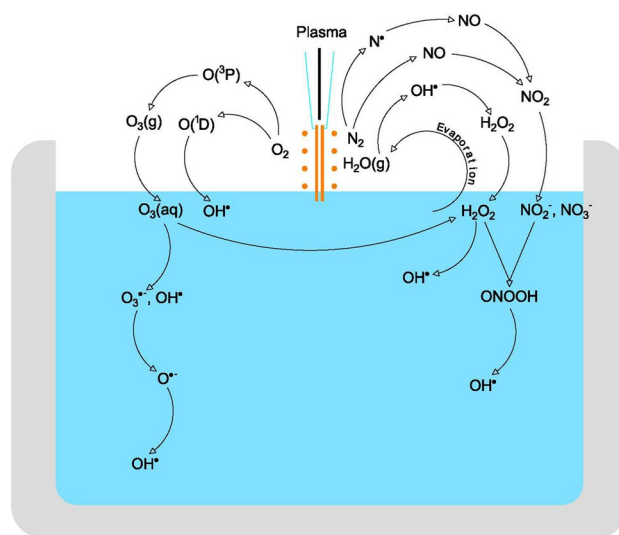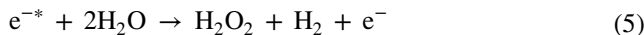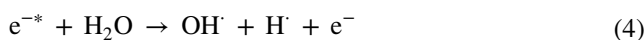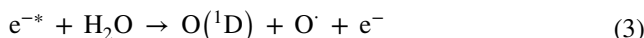|		
$OH^{\cdot} + H^+ + e^- \rightarrow H_2O$	E^0_{OH/H_2O}	2.85 V
$O^{\cdot} + 2H^+ + 2e^- \rightarrow 2H_2O$	E^0_{O/H_2O}	2.42 V
$O_3 + 2H^+ + 2e^- \rightarrow O_2 + H_2O$	$E^0_{O_3/O_2}$	2.07 V
$H_2O_2 + 2H^+ + 2e^- \rightarrow 2H_2O$	$E^0_{H_2O_2/H_2O}$	1.77 V
$O_2 + 4H^+ + 4e^- \rightarrow 2H_2O$	$E^0_{O_2/H_2O}$	1.23 V

Fig. 2 Important chemical species in the gas and liquid phase induced by Ar fed plasma needle discharge

$$e^{-*} + H_2O \rightarrow O(^1D) + O^{\cdot} + e^- \tag{3}$$

$$e^{-*} + H_2O \rightarrow OH^{\cdot} + H^{\cdot} + e^- \tag{4}$$

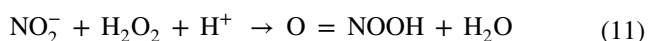$$e^{-*} + 2H_2O \rightarrow H_2O_2 + H_2 + e^- \tag{5}$$

Further important reactions related to the formation of the primary long live reactive species (O_3, H_2O_2, NO_3^-, NO_2^-) and their dissolution in water are described below. $O^{\cdot}$ generated in air plasma together with O_2 produce O_3 which reacting with water molecules forms H_2O_2 (Eqs. 6–7). Additional H_2O_2 generation mechanism is through the recombination reaction of $OH^{\cdot}$ radicals (Eq. 8).

$$O^{\cdot} + O_2 + M \rightarrow O_3 + M$$
$$(M - \text{third collision partner, which may be Ar, } O_2, N_2, \text{ etc.})$$
$$\tag{6}$$

$$O_3 + H_2O \rightleftharpoons O_2 + H_2O_2 \tag{7}$$

$$OH^{\cdot} + OH^{\cdot} \rightarrow H_2O_2 \tag{8}$$
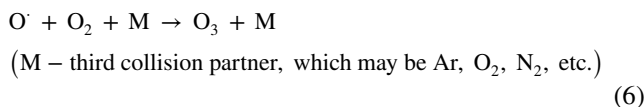
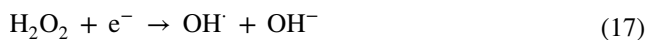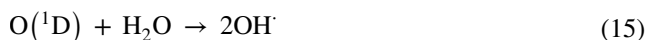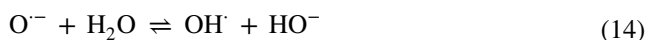Nitrogen oxides (NO, NO_2) formed in air plasma through reactions between O_2 and N_2 dissolve in the solution creating nitrites and nitrates (Eqs. 9–10) and consequently forming the peroxynitrous acid through the reaction of nitrites with hydrogen peroxide (Eq. 11) [32].

$$2NO_2 + H_2O \rightarrow NO_2^- + NO_3^- + 2H^+ \tag{9}$$

$$NO + NO_2 + H_2O \rightarrow 2NO_2^- + 2H^+ \tag{10}$$

$$NO_2^- + H_2O_2 + H^+ \rightarrow O = NOOH + H_2O \quad (11)$$
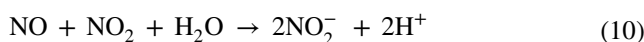
Occurrence of even more reactive species (OH·, O·, NO$_2$·etc.) (Eqs. 12–18) can be expected as well, but because of their short lifetime they can react directly with a pollutant only in its current encirclement where the reaction occurs [5, 48, 49]. Among them, the most influential reactive species found in electric discharges is OH·. It is a very powerful oxidizing agent with a standard reduction potential of $E^0 = 2.8$ V [50] and lifetime (≈ 200 µs in the gas phase and 10^{-9} s in an aqueous solution).Although it has very short lifetime there are additional OH· formation mechanisms in the bulk as a consequence of the transformation of above–mentioned long lifetime species. Several mechanisms are responsible for the OH· formation: electron impacts dissociation of H$_2$O (Eq. 4); ozone dissolution in water [51] (Eqs. 12–14); reactions of excited O atoms and O· with water (Eqs. 15, 16); reaction of e$^-$and H$_2$O$_2$ (Eq. 17) or via reaction of peroxynitrous acid in water (Eq. 18).

$$O_3 + HO^- \rightarrow O_3^{\cdot-} + OH^\cdot \quad (12)$$

$$O_3^{\cdot-} \rightarrow O^{\cdot-} + O_2 \quad (13)$$

$$O^{\cdot-} + H_2O \rightleftharpoons OH^\cdot + HO^- \quad (14)$$

$$O(^1D) + H_2O \rightarrow 2OH^\cdot \quad (15)$$

$$O^\cdot + H_2O \rightarrow 2OH^\cdot \quad (16)$$

$$H_2O_2 + e^- \rightarrow OH^\cdot + OH^- \quad (17)$$

$$O = NOOH \rightleftharpoons NO_2^\cdot + OH^\cdot \quad (18)$$

The degradation of dyes is mainly attributed to the attack of these oxidative species, which are among the most influential reactive species found in electric discharges [52] that initially attack the most sensitive chromophore group (–N = N–). The decolorization process of RO16 usually manifests as decrease of the 494 nm band intensity, relatively faster than for other bands. Therefore, it can be concluded that reactive species like OH· initially attack the chromophore group (–N = N–) followed by the degradation of aromatic part, benzene and naphthalene rings, of the dye molecule [38].

The OH· addition to the –N = N– bond probably produces the hydrazyl type radical forms, –·N–N(OH)– as reported in the literature [5], leading to the destruction of the colour in the visible range and finally mineralization into totally innocuous gaseous nitrogen [38]. The oxidation of nitrogen containing organic molecules leading to the NO$_x$ generation is also reported [53], but in small quantities not harmful for the environment.

Influence of Different Flow Rates and Composition of Feed Gas on the Decolourisation Rate

The absorption spectral changes of RO 16 solution at different irradiation time during PT with Ar as feed gas (1 slm), are presented in Fig. 3. The intensity of absorption peaks in the visible region (494 and 386 nm), as well as the intensity of peaks in the ultraviolet region (297 and 254 nm), rapidly decreased in the initial stage of the PT and after 90 min none of the absorption peaks were observed.

The kinetics of RO 16 decolourisation under PT process at different flow rates of Ar is given in Fig. 4. C_0 and C_t represent the initial dye concentration and the dye concentration at reaction time t. The RO 16 concentration of each treated sample was determined using a calibration curve which is

Fig. 3 Absorbance spectra of RO 16 for different PT times by using Ar(1slm) as feed gas
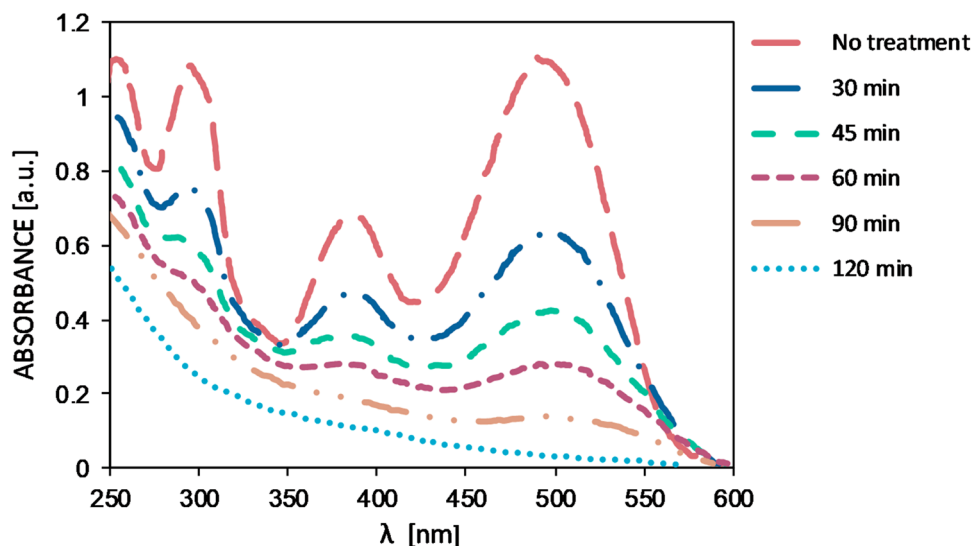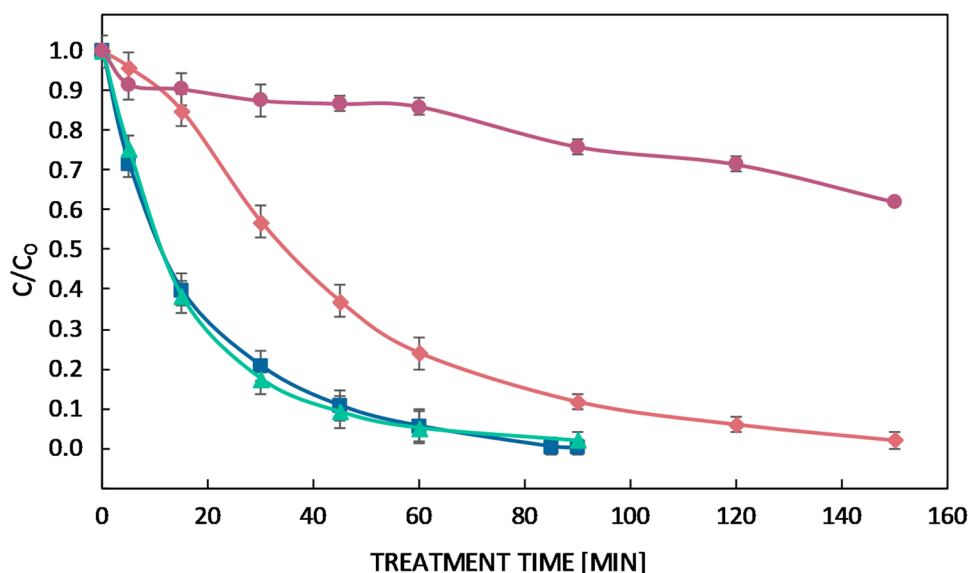
Fig. 4 Decolourisation of RO 16 (c = 50 mg/L, V = 25 mL) under PT treatment using Ar (1 and 4 slm); Ar/O$_2$ (1 slm) and Ar (4 slm + Quartz) as feed gas. Symbols: filled diamond- Ar 1 slm; filled rectangle- Ar 4 slm; filled triangle- Ar/O$_2$ 1 slm; filled circle – 4 slm with Quartz

previously established with prepared standards and theirs related absorbances. It can be observed that RO 16 decolourisation was faster for the increased flow rate of Ar (4 slm) and almost total decolourisation was achieved after 90 min. It is obvious that generation of radicals in plasma depends on gas flow rate. The higher is the flow rate, the faster is the decolourisation. However, the efficiency of radicals generation and plasma chemistry can be also tailored by changing the feed gas composition. For that purpose, in Fig. 4 is presented the kinetics of RO 16 decolourisation when 10% O$_2$ was introduced into Ar flow rate of 1 slm.

The O$_2$ introduction into the feed gas has the similar decolourisation effect on RO 16 as increasing of Ar flow rate from 1 to 4 slm. It is evident that adding only 10% O$_2$ to the feed gas (Ar, 1slm) the decolourisation of RO 16 is faster, reaching almost complete decolourisation after 90 min.

The introduction of O$_2$ into the feed gas evidently influenced the oxidation process kinetics. The better efficiency of the RO 16 oxidation with the addition of O$_2$ can be a consequence of at least two reasons. The most apparent reason is that higher amount of active species, like OH$^{\cdot}$, can be formed when O$_2$ is introduced in Ar because of the lower energy of the first ionization of O$_2$ (12.1 eV) compared to Ar (15.8 eV). In their work, Gumuchian et al. [24] measured amount of OH$^{\cdot}$ in different compositions of feed gases and concluded that in Ar/O$_2$ feed gas mixture, the concentration of OH$^{\cdot}$ was the highest [24]. Beside this, atomic oxygen can react directly with organic pollutants, and together with O$_2$ can produce very reactive ozone (Eq. 6). Nevertheless, in the paper of Miyazaki et al. [54] it was shown that very small amount of ozone was produced if the Ar concentration in Ar/O$_2$ feed gas mixture is equal or higher than 80%. Since in our experiments 90% of Ar, was used, we suppose that ozone contribution in these experiments is not of great importance. Evidently, the presence of O$_2$ in the feed gas significantly improves the oxidation potentials of plasma needle, presumably due to the formation of more reactive species (Eqs. 2, 15–16).

In order to investigate an isolated effect of plasma generated UV light on dye oxidation, the quartz glass was placed between plasma source and RO 16 solution to block plasma–generated species from reaching the surface, allowing only UV light to pass to the sample. Namely, for 1 slm of Ar flow rate there was no observed UV contribution, while for 4 slm Ar flow rate UV dependent decolourisation was less than 15% after 60 min of treatment. For that reason, it can be concluded that isolated UV light cannot be considered as significant contributing factor to decolourising process of the dye.

Effects of the Heterogeneous Photocatalysis on the RO 16 Removal

Among the semiconductors, titanium dioxide (TiO$_2$) is by far the most frequently studied photocatalyst, highly abundant in nature, photochemically very stable under ambient conditions and environmentally friendly. Among the three TiO$_2$ crystal phases: anatase, rutile and brookite, the anatase is the most frequently applied photocatalyst showing excellent photocatalytic activity, although its application is restricted to the utilization of UV light due to the large band gap (E$_g$ ~ 3.2 eV).

The photochemical decolorization of RO 16 was studied by heterogeneous photocatalysis, using anatase TiO$_2$ nanopowders as catalyst and UV lamp as an excitation source. TiO$_2$ nanopowders were synthesized by sol–gel method and the XRPD pattern of TiO$_2$ is presented in Fig. 5a.

The main diffraction peaks correspond to the anatase crystallite phase (PDF card 782,486) and no other phases were detected. Characteristic Miller indices are denoted for the main diffraction peaks. The average crystallite size, <D> and average lattice strain of the prepared sample were calculated using Williamson–Hall Method and are presented in Table 2 together with cell parameters [55].

To determine the surface area of synthesized nanopowder the nitrogen adsorption–desorption isotherm at 77 K has been measured and shown in Fig. 5b. Prior to adsorption, the sample was outgassed for 1 h under vacuum at room temperature, and additionally for 16 h at 110 °C at the same residual pressure. The specific surface areas (S_{BET}) of sample is calculated from the linear part of the adsorption isotherm by applying the Brunauer-Emmet-Teller (BET) equation [56]. The curves may be interpreted as type IV [57], typical for mesoporous materials, with an H2-type hysteresis loop,

Table 2 The unit cell parameters, average crystallite size <D> and micro strain values of TiO_2

Sample name	Unit cell parameters a, c (Å)	Williamson–Hall method	
		<D> (nm)	Microstrain (%)
TiO_2	$a = 3.784(3)$ $c = 9.53(0)$	24	0.301

indicating the presence of pore networks. The reported value of the BET specific surface area (S_{BET}) is 52 m^2 g^{-1}.

TiO_2 nanoparticles produced by sol–gel method are not porous itself, so the porous structure originates from interparticle voids. From the FE-SEM images given in the Fig. 5c, d, it is clear that we are dealing with spherical and agglomerated nonporous nanoparticles, where the particle size ranges from 30 to 100 nm.
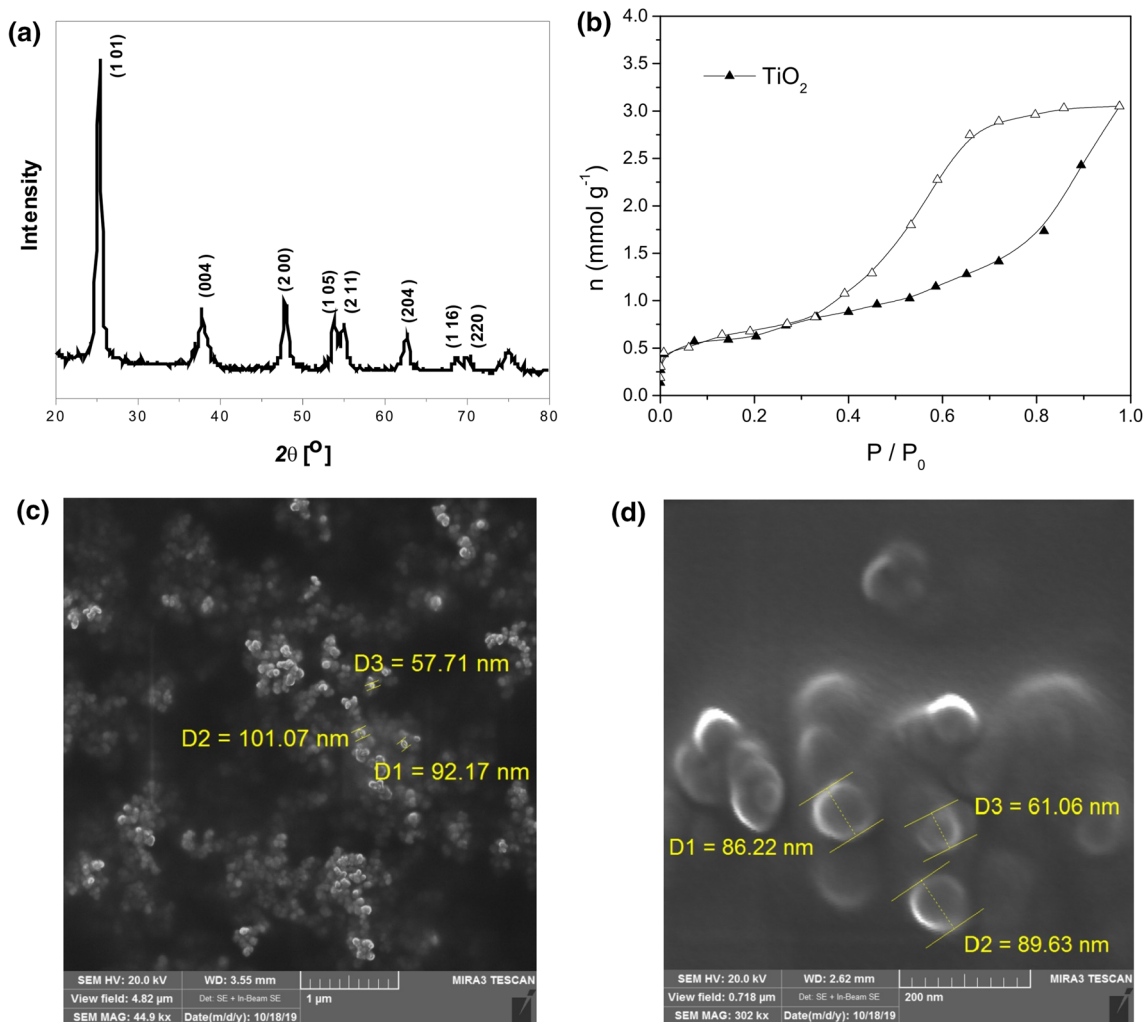

Fig. 5 XRPD pattern of TiO_2 nanopowder obtained by the sol–gel method (**a**); The nitrogen adsorption–desorption isotherm of synthesized TiO_2 nanopowder at 77 K (**b**); FE-SEM images of TiO_2 sample (**c**), (**d**)

When the RO 16–TiO_2 solution is illuminated with UV irradiation, main processes, which take place on the nanoparticles surface are illustrated in Fig. 6.

When TiO_2 solution is illuminated with light having energy greater than the band gap of the semiconductor, photogenerated electron (e_{cb}^-) –hole (h_{vb}^+) pairs are formed (Eq. 19). These pairs can be recombined within the bulk of the material or at the particle surface. Furthermore, the (e_{cb}^-) and (h_{vb}^+) can migrate to the semiconductor surface [38, 58] and react with adsorbed reactants leading to increased photocatalytic efficiency. The photodegradation mechanism can be summarized as follows:

$$TiO_2 + h\nu \xrightarrow{energy} e_{cb}^- + h_{vb}^+ \tag{19}$$

$$e_{cb}^- + h_{vb}^+ \rightarrow thermal\ energy \tag{20}$$

$$h_{vb}^+ + dye \rightarrow oxidation\ of\ organic\ molecule \tag{21}$$

$$h_{vb}^+ + H_2O \rightarrow H^+ + OH^. \tag{22}$$

$$h_{vb}^+ + OH^- \rightarrow OH^. \tag{23}$$

$$e_{cb}^- + O_2 \rightarrow O_2^- \tag{24}$$

The direct oxidation of organic substances is possible since the holes (h_{vb}^+) have high oxidative potential (Eq. 21), or they can also react with H_2O (Eq. 22) and OH^- (Eq. 23) producing very active and unselective $OH^.$ radicals [14, 38, 58]. On the other hand, photogenerated electrons can react with O_2 molecules dissolved in water forming superoxide

radical anion ($O_2^{.-}$) (Eq. 24) leading to the production of other very reactive species as follows:

$$O_2^- + H^+ \rightarrow HO_2^. \tag{25}$$

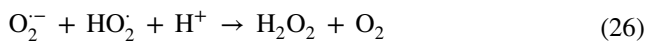$$O_2^- + HO_2^. + H^+ \rightarrow H_2O_2 + O_2 \tag{26}$$

Figure 7 shows the decolourisation rate of RO 16 for TiO_2 nanopowder activated by UV lamp. As can be seen from Fig. 7, photodegradation of the dye reached about 90% after 90 min of treatment, similar to the decolourisation effects of plasma needle for Ar 1 slm (Fig. 4). No detectable degradation of RO 16 was registered without the presence of TiO_2 sample (triangles on Fig. 7).

The presence of H_2O and O_2 molecules is crucial for generation of very reactive radicals. In the presence of H_2O and O_2 molecules, highly reactive radicals such as $OH^.$, $O_2^{.-}$ and $HO_2^.$, generated through processes of photodegradation, substantially contribute to the degradation of organic molecules/pollutants. However, the most important contribution and benefits among these processes arise from reactions accompanying generation of hydroxyl radicals. These radicals are considered as very strong and nonselective oxidizing species [59, 60]. The presence of functional groups at the surface of TiO_2 affects the formation of hydroxyl radicals. Infrared spectroscopy is used to analyse the surface of TiO_2. The IR spectrum of TiO_2 nanopowder is presented in Fig. 8a in the range from 500 to 4000 cm^{-1}. The main bands of O−H groups and H_2O are denoted with arrows. Namely, a wide band around ~ 3400 cm^{-1}, corresponds to stretching vibration of the O−H bond involved in hydrogen bonding O−H···O, whereas the band around ~ 1600 cm^{-1} can be ascribed to the bending mode of the water molecules H−O−H.

Fig. 6 Formation of e^-/h^+ pars in TiO_2 nanoparticles and catalytic processes on TiO_2 surface

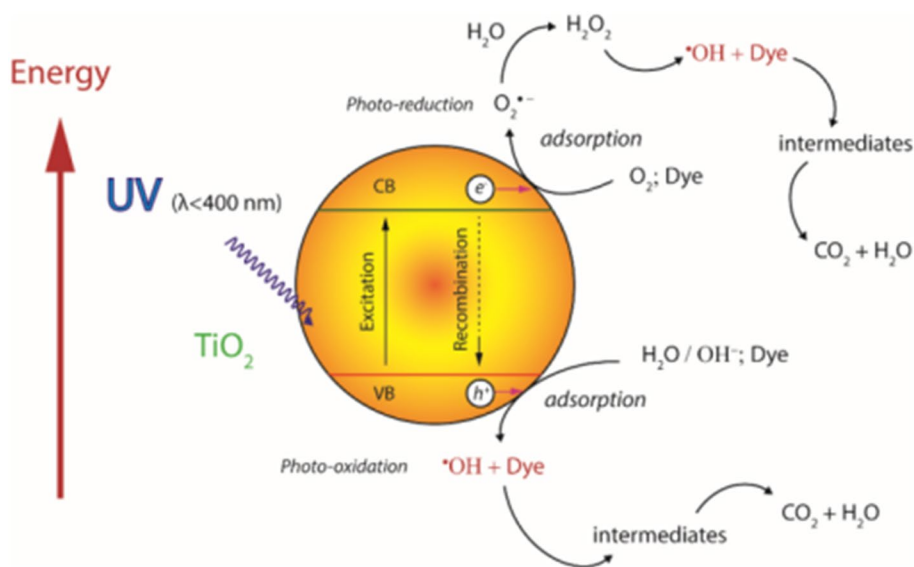**Fig. 7** Decolourisation efficiency of RO 16 (c = 50 mg/l, V = 25 ml) by using TiO$_2$ (c = 2 g/l) under UV irradiation. Symbols: filled circle- RO 16 + UV + TiO$_2$; filled triangle RO 16 + UV
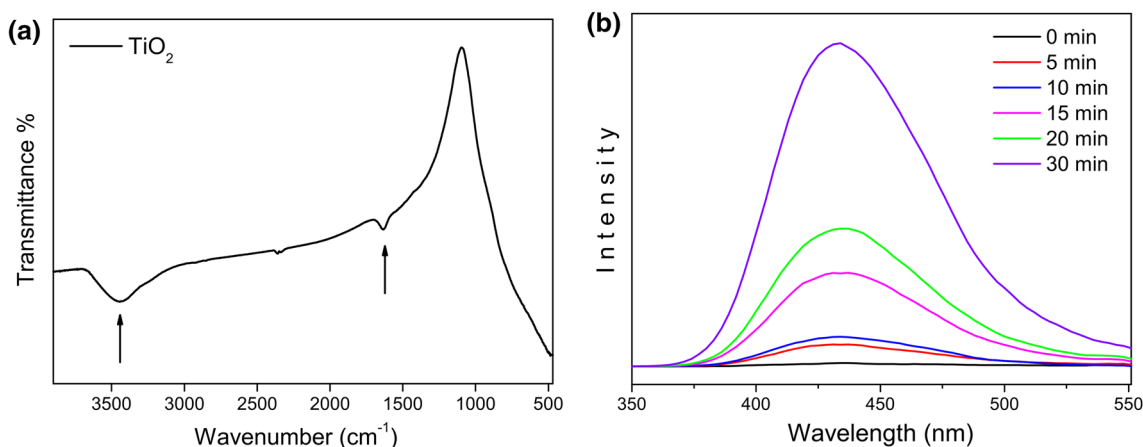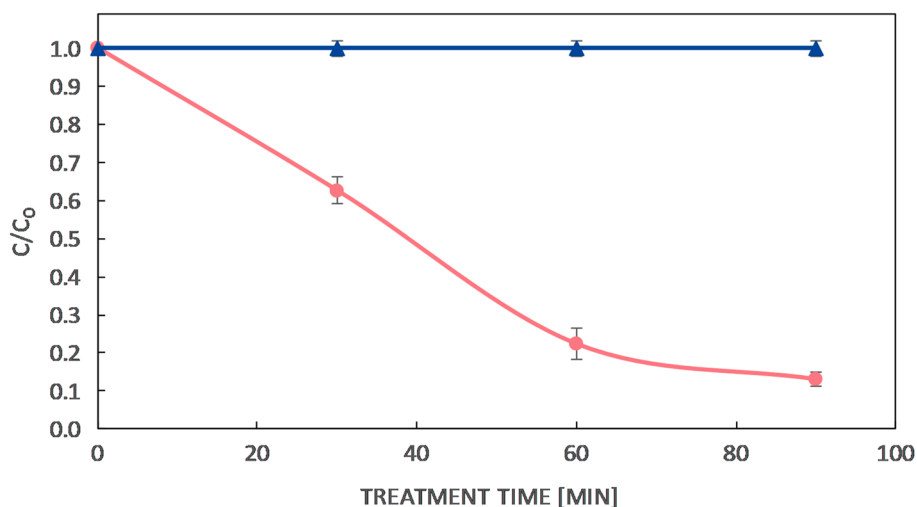

Fig. 8 IR spectrum of TiO$_2$ nanopowder (**a**), PL spectral changes of a TA–OH solution generated by TiO$_2$ under UV light irradiation (**b**)

The IR spectrum confirmed existence of O−H groups and water molecules (H$_2$O), on the surface of TiO$_2$ nanopowder (Fig. 8a), implying that generation of OH$^{\cdot}$ radicals in high concentration is likely to occur.

Since the hydroxyl radicals are considered the primary oxidizing species their presence on the surface of the UV illuminated photocatalyst can be confirmed in reaction with terephthalic acid (TA) as a probe molecule. This acid reacts with OH$^{\cdot}$ radicals, generated at the water/TiO$_2$ interface, forming a highly fluorescent product: 2-hydroxy-terephthalic acid (TA-OH), with intensive peak at about 425 nm [61]. Since PL peak intensity is proportional to the amount of generated OH$^{\cdot}$ radicals, by monitoring the changes in the intensity of 425 nm peak the hydroxyl radicals could be detected indirectly. From the Fig. 8b, it can be observed that the intensity of 425 nm peak increases in time, meaning that the concentration of hydroxyl radicals also increases [61, 62]. The spectrum labelled as "0 min" represents the pure TA solution recorded prior the UV

irradiation source. These results clearly demonstrated that with increasing illumination time the increasing amount of OH$^{\cdot}$ radicals are formed at TiO$_2$/water interface, responsible for dye degradation.

Effects of the Plasma–Tio$_2$ Catalyst Treatment on the RO 16 Removal

Figure 9 illustrates the degradation kinetics of RO 16 during the combined TiO$_2$ and non–thermal plasma treatment—PC treatment. As can be seen from Fig. 9, PC treatment is more efficient than PT (Fig. 4) for the same Ar flow rate of 1 slm. Namely, after 15 min more than 40% of dye was degraded under the PC treatment, whereas under PT the photodegradation of dye reached only 15%. It is also evident that the time for complete decolourisation reduced from 150 to 120 min. Similar effect was observed with increased feed gas flow rate (4 slm) when the time for complete RO 16 decolourisation was shortened from 90 min (PT) to 60 min (PC). Improved

Fig. 9 Decolourisation of RO 16 (c = 50 mg/L, V = 25 mL) under PC treatment by using TiO$_2$ (c = 2 g/L) and Ar (1, 4 slm) as feed gas. Symbols: filled diamond- Ar 4 slm + Quartz + TiO$_2$; filled rectangle- Ar 1 slm + TiO$_2$; filled triangle- Ar 1 slm + Quartz + TiO$_2$; filled circle –Ar 4 slm + TiO$_2$
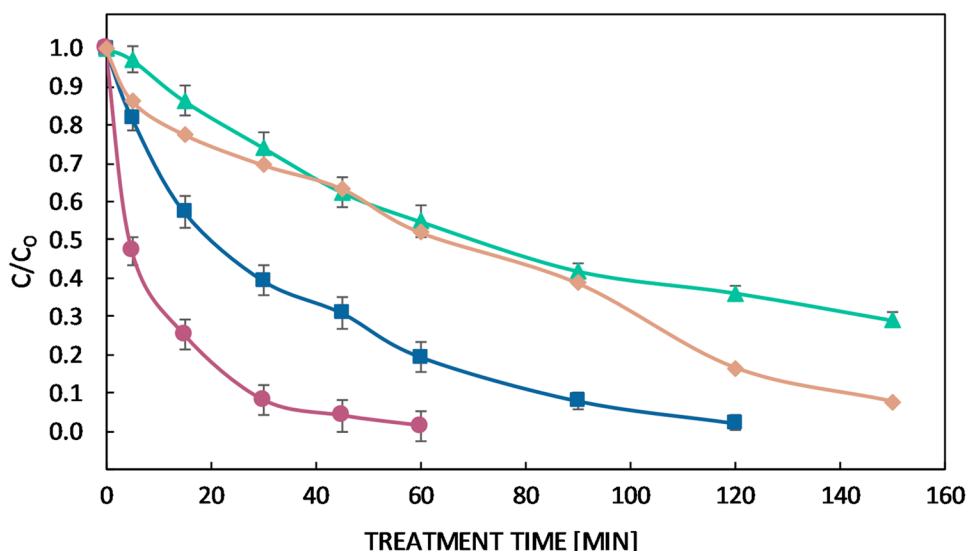
decolourization of RO 16 can be ascribed to the synergic effect of plasma–photocatalysis process.

In order to investigate an isolated effect of plasma generated UV light on dye degradation during the PC treatment, we placed a quartz glass between plasma source and TiO$_2$–dye solution, allowing only UV light to pass to the solution. From Fig. 9 it is evident that the dye degradation process was much slower compared to the PC experiment without quartz glass. Hence, it is clear that UV emission from the plasma needle activates TiO$_2$ leading to enhanced synergic effects for pollutant removal.

The oxygen addition (10%) to the feed gas (1 slm of Ar) further improved the PC decolourisation process, i.e. the synergic effect between plasma and photocatalyst was more pronounced, as the total decolourisation was achieved after 60 min (Fig. 10).

The experimental kinetic data for all presented treatments followed pseudo first–order kinetics and were fitted by pseudofirst–order reaction, $ln(C/C_o) = kt$ where k is pseudo–first order constant rate, t the treatment time. The constant rates and correlation coefficient (R^2) for different treatment setups (PT, heterogenous photocatalysis and PC) are presented in Table 3.

In the case of PT treatment, with increasing Ar flow rate from 1 to 4 slm, the constant rate k increases from 24.5 to 51.8×10^{-3} min^{-1}. The k values for Ar 4 slm ($k = 51.8 \times 10^{-3}$ min^{-1}) and mixture of Ar/O$_2$ 1 slm ($k = 47.4 \times 10^{-3}$ min^{-1}) are comparable implying similar final oxidation effect. PT treatment with Ar 1 slm (k = 24.5×10^{-3} min^{-1}) manifest almost the same oxidation degree as heterogeneous photocatalysis (k = 22.8×10^{-3} min^{-1}). This is very important knowing that

Fig. 10 Decolourisation of RO 16 (c = 50 mg/L, V = 25 mL) under the PC treatment using TiO$_2$ (c = 2 g/L) and Ar (1slm) and Ar/O$_2$ (1slm) as feed gas. Symbols: filled diamond- Ar/O$_2$ 1 slm + TiO$_2$; filled rectangle- Ar 1 slm + TiO$_2$
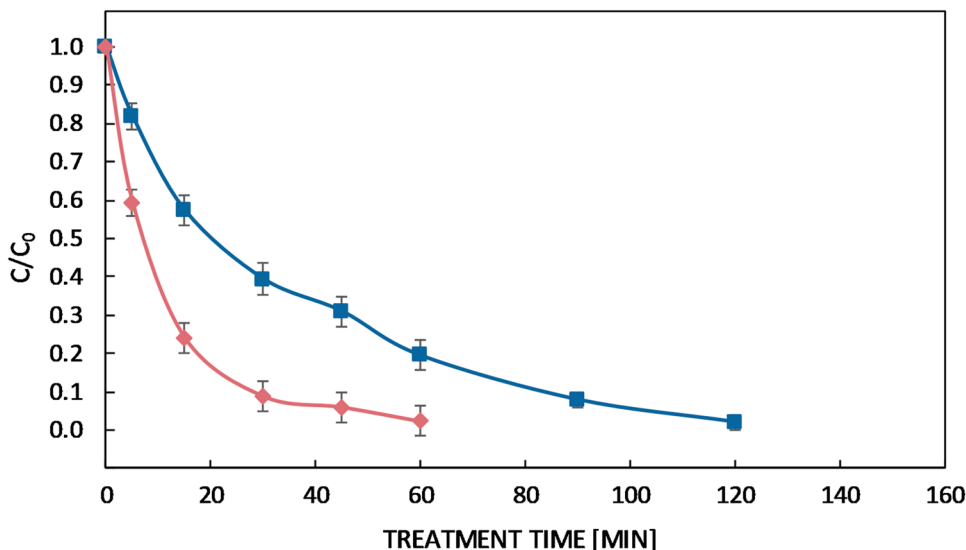
Table 3 Constant rates for different treatment setups

Treatment setups		Constant rates, $k \times 10^{-3} (min^{-1})$	R^2
PT	1 slm (Ar)	24.5	0.988
PT	4 slm (Ar)	51.8	0.993
PT	1 slm (Ar/O_2)	47.4	0.970
HP	TiO$_2$ + UV 300 W	22.8	0.975
PC	1 slm (Ar) + TiO$_2$	30.1	0.986
PC	1 slm (Ar/O_2) + TiO$_2$	66.2	0.953
PC	4 slm (Ar) + TiO$_2$	73.1	0.971
PC with quartz	1 slm (Ar) + TiO$_2$ + Quartz	8.9	0.986
PC with quartz	4 slm (Ar) + TiO$_2$ + Quartz	15.5	0.943

plasma needle needs smaller power consumption for TiO$_2$ activation than UV lamp.

In the case of PT treatment with quartz glass, the UV radiation emitted from the 1 slm plasma needle was not enough to decolourise RO 16 dye by itself. For increased Ar flow rate (4 slm) low value of constant rate ($k = 3.1 \times 10^{-3}$ min^{-1}) confirmed that UV light cannot be considered as significant factor during the process of decolourisation.

As expected, the best removal efficiency was obtained with combined plasma/TiO$_2$ process (PC). Namely, among all experiments with different setups (HP, PT and PC), the PC rate constants are the highest (see Table 3).

This is particularly evidenced for increased Ar flow rate (4 slm) when the rate constant is almost 50% higher for PC than for PT treatment ($k = 73.1 \times 10^{-3}$ min^{-1} vs. $k = 51.8 \times 10^{-3}$ min^{-1}). Therefore, it can be concluded that the synergic effect of two AOPs is evident and very dependent on the flow rate of feed gas and gas mixture. PC experiment with quartz glass demonstrated that UV radiation from the plasma needle source evidently has influence on the TiO$_2$ photolytic activity and contribute to the RO 16 decolourisation process. Further investigations will be directed to the estimation of the optimal TiO$_2$ concentration, identification of RO 16 oxidation by–products and determination of their levels of toxicity.

Conclusions

In this paper, we investigated the RO 16 decolourisation process by using two advanced oxidation processes (plasma discharge process and heterogenous photocatalysis), as well as combined plasma/TiO$_2$ process. For that purpose, we have developed a low power atmospheric pressure plasma source (plasma needle). The anatase TiO$_2$ nanopowders, used in experiments, were synthetized by sol–gel method. In the case of only plasma treatment, it was demonstrated that both flow rate and feed gas composition had significant effect on

dye removal. The presence of O$_2$ in the feed gas, as well as, increased feed gas flow rate significantly improved the process of RO16 decolourisation as compared with the TiO$_2$ based heterogenous photocatalysis.

The RO 16 degradation efficiency significantly improved when plasma was combined with TiO$_2$ photocatalyst. Such an improvement can be attributed to synergic effects of radicals generated by the plasma in the gas phase and delivered to the liquid and radicals generated directly in the liquid on the surface of TiO$_2$. The synergic effect of two AOPs was more pronounced at higher flow rate of the plasma feeding gas. Accordingly, we can conclude that simultaneous application of different AOPs can offer better solution for wastewater treatment and improves energy utilization efficiency when using plasma needle as UV source.

Compliance with Ethical Standards

Conflict of interest The authors declare that they have no conflict of interest.

References

1. Bizani, E., Fytianos, K., Poulios, I., Tsiridis, V.: Photocatalytic decolorization and degradation of dye solutions and wastewaters in the presence of titanium dioxide. J. Hazard. Mater. **136**, 85–94 (2006)
2. de Lima, R.O.A., Bazo, A.P., Salvadori, D.M.F., Rech, C.M., de Palma, O.D., de Aragão, U.G.: Mutagenic and carcinogenic potential of a textile azo dye processing plant effluent that impacts a drinking water source. Mutat. Res. Genet. Toxicol. Environ. Mutagen. **626**(1–2), 53–60 (2007)
3. Gao, J., Zhang, Q., Su, K., Chen, R., Peng, Y.: Biosorption of Acid Yellow 17 from aqueous solution by non-living aerobic granular sludge. J. Hazard. Mater. **174**, 215–225 (2010)
4. Dutta, S., Saha, R., Kalita, H.: Rapid reductive degradation of azo and anthraquinone dyes by nanoscale zero-valent iron. Environ. Technol. Innov. **5**, 176–187 (2016)
5. Dojčinović, B.P., Roglić, G.M., Obradović, B.M., Kuraica, M.M., Kostić, M.M., Nešić, J., Manojlović, D.D.: Decolorization of reactive textile dyes using water falling film dielectric barrier discharge. J. Hazard. Mater. **192**, 763–771 (2011)
6. Chandanshive, V.V., Kadam, S.K., Khandare, R.V., Kurade, M.B., Jeon, B.H., Jadhav, J.P., Govindwar, S.P.: In situ phytoremediation of dyes from textile wastewater using garden ornamental plants, effect on soil quality and plant growth. Chemosphere **210**, 968–976 (2018)
7. Pandey, A., Singh, P., Iyengar, L.: Bacterial decolorization and degradation of azo dyes. Int. Biodeterior. Biodegrad. **59**, 73–84 (2007)
8. Ghezzar, M.R., Abdelmalek, F., Belhadj, M., Benderdouche, N., Addou, A.: Enhancement of the bleaching and degradation of

textile wastewaters by Gliding arc discharge plasma in the presence of TiO2 catalyst. J. Hazard. Mater. **164**(2–3), 1266–1274 (2009)

9. Tichonovas, M., Krugly, E., Racys, V., Hippler, R., Kauneliene, V., Stasiulaitiene, I., Martuzevicius, D.: Degradation of various textile dyes as wastewater pollutants under dielectric barrier discharge plasma treatment. Chem. Eng. J. **229**, 9–19 (2013)

10. Tijani, J.O., Fatoba, O.O., Madzivire, G., Petrik, L.F.: A review of combined advanced oxidation technologies for the removal of organic pollutants from water. Water Air Soil Pollut. **225**(9), 2102 (2014)

11. Foster, J.E.: Plasma-based water purification: challenges and prospects for the future. Phys. Plasmas **24**(5), 055501 (2017)

12. Wang, T., Qu, G., Ren, J., Sun, Q., Liang, D., Hu, S.: Organic acids enhanced decoloration of azo dye in gas phase surface discharge plasma system. J. Hazard. Mater. **302**, 65–71 (2016)

13. Mijin, D., Radulovic, M., Zlatic, D., Jovancic, P.: Photocatalytic degradation of textile dye RO 16 in TiO_2 water suspension by simulated solar light. Chem. Ind. Chem. Eng. Q. **13**, 179–185 (2007)

14. Mijin, D., Zlatic, D., Uscumlic, G., Jovancic, P.: Solvent effects on photodegradation of CI reactive orange 16 by simulated solar light. Hem. Ind. **62**, 275–281 (2008)

15. Khan, M.A.N., Siddique, M., Wahid, F., Khan, R.: Removal of reactive blue 19 dye by sono, photo and sonophotocatalytic oxidation using visible light. Ultrason. Sonochem. **26**, 370–377 (2015)

16. Basturk, E., Karatas, M.: Advanced oxidation of Reactive Blue 181 solution: a comparison between Fenton and Sono-Fenton process. Ultrason. Sonochem. **21**, 1881–1885 (2014)

17. Becelic-Tomin, M., Dalmacija, M., Dalmacija, B., Rajic, L., Tomasevic, D.: Degradation of industrial azo dye in aqueous solution by heterogeneous Fenton process (fly ash/H_2O_2). Hem. Ind. **66**, 487–496 (2012)

18. Jiang, B., Zheng, J., Qiu, S., Wu, M., Zhang, Q., Yan, Z., Xue, Q.: Review on electrical discharge plasma technology for wastewater remediation. Chem. Eng. J. **236**, 348–368 (2014)

19. Lukes, P., Clupek, M., Babicky, V., Janda, V., Sunka, P.: Generation of ozone by pulsed corona discharge over water surface in hybrid gas—liquid electrical discharge reactor. J. Phys. D **38**, 409–416 (2005)

20. Sun, Y., Liu, Y., Li, R., Xue, G., Ognier, S.: Degradation of reactive blue 19 by needle-plate non-thermal plasma in different gas atmospheres: kinetics and responsible active species study assisted by CFD calculations. Chemosphere **155**, 243–249 (2016)

21. McKay, K., Salter, T.L., Bowfield, A., Walsh, J.L., Gilmore, I.S., Bradley, J.W.: Comparison of three plasma sources for ambient desorption/ionization mass spectrometry. J. Am. Soc. Mass Spectrom. **25**, 1528–1537 (2014)

22. Dünnbier, M., Schmidt-Bleker, A., Winter, J., Wolfram, M., Hippler, R., Weltmann, K.D., Reuter, S.: Ambient air particle transport into the effluent of a cold atmospheric-pressure argon plasma jet investigated by molecular beam mass spectrometry. J. Phys. D **46**(43), 435203 (2013)

23. Puač, N., Maletić, D., Lazović, S., Malović, G., Dordević, A., Petrović, Z.L.: Time resolved optical emission images of an atmospheric pressure plasma jet with transparent electrodes. Appl. Phys. Lett. **101**(2), 024103 (2012)

24. Gumuchian, D., Cavadias, S., Duten, X., Tatoulian, M., Da Costa, P., Ognier, S.: Organic pollutants oxidation by needle/plate plasma discharge: on the influence of the gas nature. Chem. Eng. Process **82**, 185–192 (2014)

25. Robert, E., Darny, T., Dozias, S., Iseni, S., Pouvesle, J.M.: New insights on the propagation of pulsed atmospheric plasma streams: from single jet to multi jet arrays. Phys. Plasmas **22**(12), 122007 (2015)

26. Ghezzar, M.R., Saïm, N., Belhachemi, S., Abdelmalek, F., Addou, A.: New prototype for the treatment of falling film liquid effluents by gliding arc discharge part I: application to the discoloration and degradation of anthraquinonic Acid Green 25. Chem. Eng. Process. **72**, 42–50 (2013)

27. Kim, H.S., Wright, K.C., Hwang, I.H., Lee, D.H., Rabinovich, A., Fridman, A.A., Cho, Y.I.: Effects of H2O2 and low pH produced by gliding arc discharge on the inactivation of Escherichia coli in water. Plasma Med. **1**(3–4), 295–307 (2011)

28. Hijosa-Valsero, M., Molina, R., Schikora, H., Müller, M., Bayona, J.M.: Removal of priority pollutants from water by means of dielectric barrier discharge atmospheric plasma. J. Hazard. Mater. **262**, 664–673 (2013)

29. Pavlovich, M.J., Chang, H.-W., Sakiyama, Y., Clark, D.S., Graves, D.B.: Ozone correlates with antibacterial effects from indirect air dielectric barrier discharge treatment of water. J. Phys. D **46**, 145202 (2013)

30. Lukes, P., Clupek, M., Babicky, V., Sunka, P.: Ultraviolet radiation from the pulsed corona discharge in water. Plasma Sources Sci. Technol. **17**, 024012 (2008)

31. Lukes, P., Aoki, N., Spetlikova, E., Hosseini, S.H.R., Sakugawa, T., Akiyama, H.: Effects of pulse frequency of input power on the physical and chemical properties of pulsed streamer discharge plasmas in water. J. Phys. D **46**, 125202 (2013)

32. Lukes, P., Dolezalova, E., Sisrova, I., Clupek, M.: Aqueous-phase chemistry and bactericidal effects from an air discharge plasma in contact with water: evidence for the formation of peroxynitrite through a pseudo-second-order post-discharge reaction of H2O2 and HNO2. Plasma Sources Sci. Technol. **23**(1), 015019 (2014)

33. Garcia-Segura, S., Brillas, E.: Applied photoelectrocatalysis on the degradation of organic pollutants in wastewaters. J. Photochem. Photobiol. C **31**, 1–35 (2017)

34. Spasiano, D., Marotta, R., Malato, S., Fernandez-Ibañez, P., Di Somma, I.: Solar photocatalysis: materials, reactors, some commercial, and pre-industrialized applications. A comprehensive approach. Appl. Catal. B **170**, 90–123 (2015)

35. Whitehead, J.C.: Plasma—catalysis: the known knowns, the known unknowns and the unknown unknowns. J. Phys. D **49**, 243001 (2016)

36. Parvulescu, V.I., Magureanu, M., Lukes, P., Liu, J., Bruggeman, P.J., et al.: Pulsed discharge purification of water containing non-degradable hazardous substances. J. Phys. D **33**, 145202 (2011)

37. Wang, T.C., Lu, N., Li, J., Wu, Y.: Plasma-TiO$_2$ catalytic method for high-efficiency remediation of p-nitrophenol contaminated soil in pulsed discharge. Environ. Sci. Technol. **45**, 9301–9307 (2011)

38. Ghezzar, M.R., Abdelmalek, F., Belhadj, M., Benderdouche, N., Addou, A.: Gliding arc plasma assisted photocatalytic degradation of anthraquinonic acid green 25 in solution with TiO2. Appl. Catal. B **72**(3–4), 304–313 (2007)

39. Evgenidou, E., Fytianos, K., Poulios, I.: Photocatalytic oxidation of dimethoate in aqueous solutions. J. Photochem. Photobiol. A **175**, 29–38 (2005)

40. Chen, L., Zhang, X., Huang, L., Lei, L.: Application of in-plasma catalysis and post-plasma catalysis for methane partial oxidation to methanol over a Fe_2O_3-CuO/γ- Al_2O_3 catalyst. J. Nat. Gas Chem. **19**, 628–637 (2010)

41. Gallon, H.J., Tu, X., Twigg, M.V., Whitehead, J.C.: Plasma-assisted methane reduction of a NiO catalyst-low temperature activation of methane and formation of carbon nanofibres. Appl. Catal. B **106**, 616–620 (2011)

42. Tu, X., Gallon, H.J., Whitehead, J.C.: Plasma-assisted reduction of a NiO/Al2O3 catalyst in atmospheric pressure H_2/Ar dielectric barrier discharge. Catal. Today. **211**, 120–125 (2013)

43. Du, Y.L., Deng, Y., Zhang, M.S.: Variable-temperature Raman scattering study on anatase titanium dioxide nanocrystals. J. Phys. Chem. Solids. **67**, 2405–2408 (2006)

44. Zaplotnik R, Kregar Z, Bišćan M, Vesel A, Cvelbar U, Mozetič M, Milošević S (2014) Multiple vs. single harmonics AC-driven atmospheric plasma jet. EPL 106(2):25001.

45. Parvulescu, V., Magureanu, M., Lukes, P.: Plasma chemistry and catalysis in gases and liquids. Wiley, New Jersey (2012)

46. Chen, Q., Li, J., Li, Y.: A review of plasma—liquid interactions for nanomaterial synthesis. J. Phys. D 48, 424005 (2015)

47. Malik, P.: Kinetics of decolourisation of azo dyes in wastewater by UV/H_2O_2 process. Sep. Purif. Technol. 36, 167–175 (2004)

48. Malik, M.A., Ghaffar, A., Malik, S.A.: Water purification by electrical discharges. Plasma Sources Sci. Technol. 10, 82–91 (2001)

49. Liu, D.X., Liu, Z.C., Chen, C., Yang, A.J., Li, D., Rong, M.Z., Chen, H.L., Kong, M.G.: Aqueous reactive species induced by a surface air discharge: heterogeneous mass transfer and liquid chemistry pathways. Sci. Rep. 6, 23737 (2016)

50. Ay, F., Kargi, F.: Advanced oxidation of amoxicillin by Fenton's reagent treatment. J. Hazard. Mater. 179, 622–627 (2010)

51. Bruggeman, P., Leys, C.: Non-thermal plasmas in and in contact with liquids. J. Phys. D 42(5), 053001 (2009)

52. Puač, N., Miletić, M., Mojović, M., Popović-Bijelić, A., Vuković, D., Miličić, B., Maletić, D., Lazović, S., Malović, G., Petrović, Z.L.: Sterilization of bacteria suspensions and identification of radicals deposited during plasma treatment. Open Chem. 13, 332–338 (2015)

53. Garcia-Segura, S., Mostafa, E., Baltruschat, H.: Could NOx be released during mineralization of pollutants containing nitrogen by hydroxyl radical? Ascertaining the release of N-volatile species. Appl. Catal. B 207, 376–384 (2017)

54. Miyazaki, Y., Satoh, K., Itoh, H.: Pulsed discharge purification of water containing nondegradable hazardous substances. Electr. Eng. Japan. 174, 1–8 (2011)

55. Williamson, G.K., Hall, W.H.: X-ray line broadening from filed aluminium and wolfram. Acta Metall. 1, 22 (1953)

56. Brunauer, S., Emmett, P.H., Teller, E.: Adsorption of gases in multimolecular layers. J. Am. Chem. Soc. 60(2), 309–319 (1938)

57. Rouquerol, J., Avnir, D., Fairbridge, C.W., Everett, D.H., Haynes, J.H., Pernicone, N., Ramsay, J.D., Sing, K.S.W., Unger, K.K.: Recommendations for the characteruzation of porous solids. Pure Appl. Chem. 66, 1739–1758 (1994)

58. Ribeiro, A.R., Nunes, O.C., Pereira, M.F.R., Silva, A.M.T.: An overview on the advanced oxidation processes applied for the treatment of water pollutants defined in the recently launched Directive 2013/39/EU. Environ. Int. 75, 33–51 (2015)

59. Daneshvar N, Rasoulifard MH, Khataee AR, Hosseinzadeh F (2007) Removal of C.I. acid orange 7 from aqueous solution by UV irradiation in the presence of ZnO nanopowder. J. Hazard. Mater. 143(1–2), 95–101.

60. Turchi, C.S., Ollis, D.F.: Photocatalytic degradation of organic water contaminants: mechanisms involving hydroxyl radical attack. J. Catal. 122, 178–192 (1990)

61. Yu, J., Wang, W., Cheng, B., Su, B.L.: Enhancement of photocatalytic activity of mesoporous TiO_2 powders by hydrothermal surface fluorination treatment. J. Phys. Chem. C 113, 6743–6750 (2009)

62. Su, T.M., Liu, Z.L., Liang, Y., Qin, Z.Z., Liu, J., Huang, Y.Q.: Preparation of PbYO composite photocatalysts for degradation of methyl orange under visible-light irradiation. Catal. Commun. 18, 93–97 (2012)

Affiliations

Tatjana Mitrović[1] · Nataša Tomić[2] · Aleksandra Djukić-Vuković[3] · Zorana Dohčević-Mitrović[4] · Saša Lazović[2]

✉ Saša Lazović
   lazovic@ipb.ac.rs

1 "Jaroslav Černi" Water Institute, Jaroslava Černog 80, 11226 Belgrade, Serbia

2 Institute of Physics Belgrade, University of Belgrade, Pregrevica 118, 11080 Belgrade, Serbia

3 Faculty of Technology and Metallurgy, University of Belgrade, Karnegijeva 4, 11000 Belgrade, Serbia

4 Nanostructured Matter Laboratory, Institute of Physics Belgrade, University of Belgrade, Pregrevica 118, 11080 Belgrade, Serbia